



Experimental investigation of shading façade-integrated solar absorber system under hot tropical climate



Khai Mun Ng^{a,c,*}, Nor Mariah Adam^a, Mohd Zainal Abidin Ab Kadir^{b,d}

^a Department of Mechanical and Manufacturing Engineering, Universiti Putra Malaysia, 43400 Serdang, Selangor, Malaysia

^b Department of Electrical and Electronic Engineering, Universiti Putra Malaysia, 43400 Serdang, Selangor, Malaysia

^c Department of Mechanical and Automotive Engineering, Infrastructure University Kuala Lumpur, 43000 Kajang, Selangor, Malaysia

^d Institute of Power Engineering (IPE), Universiti Tenaga Nasional, Jalan IKRAM-UNITEN, 43000 Kajang, Selangor, Malaysia

ARTICLE INFO

Keywords:

Shading façade-integrated solar absorber
Hot tropical climate
Temperature
Efficiency

ABSTRACT

In this paper, a shading façade-integrated solar absorber system has been assessed outdoors under the hot tropical climate. The system was developed, and its performance was tested for 79 days under a standard system operating condition. The outdoor field test has demonstrated that the system was principally dependent on the available global irradiance, and its performance was impaired by the high occurrence of afternoon rain. On average, the system was capable to achieve a daily efficiency of 50.5%, maximum daily water temperature attained at 48.9 °C, and solar water heating rate of 2.9 °C/h. Findings showed that the system could perform most frequently at a daily efficiency ranging from 45% to 60%, and the maximum daily water temperature attained from 45 °C to 57 °C during the test period. Empirical results indicate that there exist several linear regressions between the variables that show acceptable correlations. An additional experiment was carried out to assess the heat distribution mapping of the experimental model.

1. Introduction

Building as the marking of human civilisation, has been identified as one of the largest energy consumers. A study shows the building sector has contributed to about 40% of the global energy expenditure due to the modern living standards [1]. Out of the total energy use in building, roughly 55% is accounted under the consumptions by heating, ventilation and air conditioning units [2]. The statistics clarifies the need of energy in building is mandatory, thus efforts to deal with energy in sustainable form to improve the thermal performance of the buildings are imperative for a green building progress.

For the building thermal loads, solar heat can be accounted into energy share in two contexts, which are solar gain attenuation and solar thermal applications. The practice of insulating the building or blocking the incident sunray has been adopted as the primary passive solution in the design stage to optimise the energy consumption. In solar heating system, solar thermal collector is ordinarily known as a reliable green product to harness the solar energy. The building integrated solar energy system attracts much attention presently due to the progress of green concept, in which the integration has been carried out on various building facades such as wall, window, roof, gutter, balcony, awning and shutter. The current trend has indicated the importance of solar

thermal integration in façade for future need in sustainable building approach [3–7].

Literature has presented the integration of solar energy model in numerous building facades to investigate its thermal performance, and its importance was reasoned. An increase of thermal collection area by this manner could compensate the limitation of a standard solar collector in the best installation position [8]. It is essential to identify an alternative position for capturing the free solar thermal as a study shows there are about 20% of the residential buildings facing architectural restraints to install the solar thermal units [9]. Besides, the adoption of solar collector integrated in building can be associated with the heat removal from building envelope by the mean of heat convection. It presents a prominent scheme for cutting down indoor cooling demand, most effectively in hot regions [10]. The integration of solar energy systems on the building could improve the insulation features, establish an active building envelope energy production in attachment to solar energy utilisation [11]. Overview the aforementioned remarks, integrating the solar thermal collection model into the building facades could possibly upgrade the façade to be multifunctional that is not merely cutting down the solar gain but producing sustainable energy source.

The existing literature mainly discussed the performance of shading

* Corresponding author at: Department of Mechanical and Manufacturing Engineering, Universiti Putra Malaysia, 43400 Serdang, Selangor, Malaysia.

E-mail addresses: mun_311@hotmail.com, ngkmun@iukl.edu.my (K.M. Ng).

<https://doi.org/10.1016/j.jobee.2019.01.031>

Received 8 March 2018; Received in revised form 24 January 2019; Accepted 24 January 2019

Available online 26 January 2019

2352-7102/ © 2019 Elsevier Ltd. All rights reserved.

Table 1
Basic dimension and configuration of prototype.

Parameters	Values
Tilt angle of solar plate	15°
Orientation of solar plate	North-facing (± 180° azimuth)
Number of solar plate	2
Length of solar plate	1125 mm
Thickness of solar plate	61 mm
Width of solar plate	429 mm
Aperture area	0.82 m ²
Gaps between two adjacent louvre plates	34.8 mm
Number of tube per solar plate	5
Horizontal extension	864 mm

devices in term of solar heat blockage for energy saving and daylight comfort, excluding the potential of energy collection from the components. Several research efforts related to the shading façade-integrated solar energy system were made [12–18]. However, most of the building integrated solar thermal models were developed and studied in higher latitude regions over 10° N [4,6,8,14,15,19–21]. Investigation in the equatorial tropics is rare despite of its attractive potential. Therefore, this is a need to assess the interaction of a shading façade-integrated solar thermal collector unit with incoming insolation under the hot tropical climate. The value of its thermal collection remains undefined quantitatively under this zone. The present work was intended to fill the gap in this scientific knowledge.

2. Experimental setup and measuring

In this work, a layout of horizontal louvre system was undertaken to be a chassis foundation for structuring the shading façade-integrated solar absorber system. The configuration of the system has been formulated to perform as a shading device and concurrently maximise the surface exposure for optimum solar radiation reception. A numerical modelling considering the geometrical and thermal models has been developed in the Universiti Putra Malaysia to design and size the system optimally. Table 1 shows the basic dimension and configuration of the shading façade-integrated solar absorber prototype. Fig. 1 depicts the technical drawing.

The system employed an active direct solar heating mechanism. The schematic view of hydraulic layout of the system in the present work is presented in Fig. 2. The layout was configured in practical and simple forms to facilitate the experimental work. The system has a check valve in the inlet cold water line to prevent the back flow, avoiding the water from flowing back into the supply line. It acted as a safety measure for unidirectional flow, in which the flow was driven by a pump. A strainer was used to filter the particles and impurities to protect the downstream hydraulic equipments and prevent the blockage inside the small absorber tubing. A flow control valve was installed in the circuit to regulate the fluid flow rate to ensure the flow was characterised under the

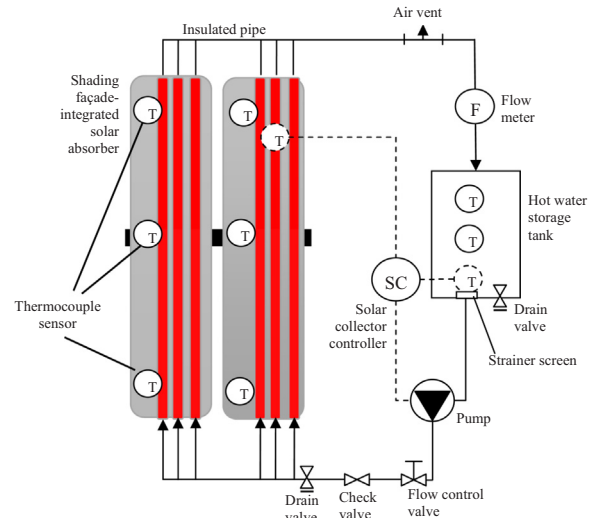


Fig. 2. Schematic view of hydraulic circuit layout of the system.



Fig. 3. View of prototype at experimental site.

intended flow regime. An automatic high temperature air vent valve was installed at the highest level of the system to allow the trapped air inside the pipe to be vented out. All the pipes outside the housing of the solar absorber unit were insulated by Superlon insulation to diminish the heat loss.

Field measurements that consisted of 79 days data reading, from May until November 2016, were examined under the standard system operating condition. There is no specific seasonal influence at the site that the weather pattern of the equatorial zone is relatively uniform throughout a typical year. The experiment has been conducted on the roof of the two-floor building located at latitude of 2°58' N, longitude of 101°44' E and elevation of 69 m. In the present work, the water heating

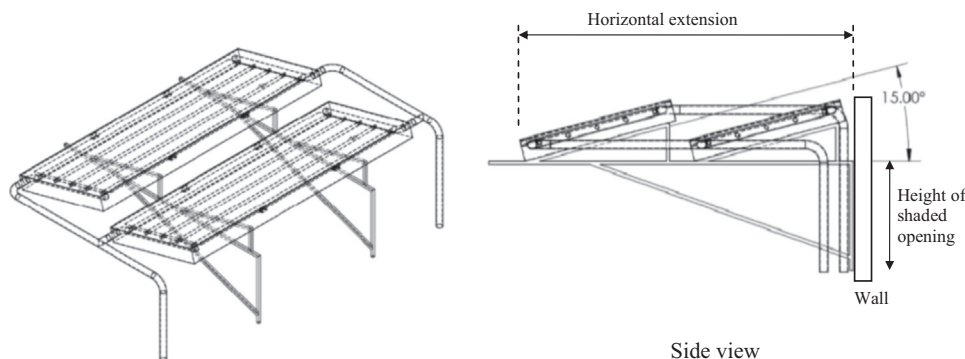


Fig. 1. Technical drawing illustrating the prototype.

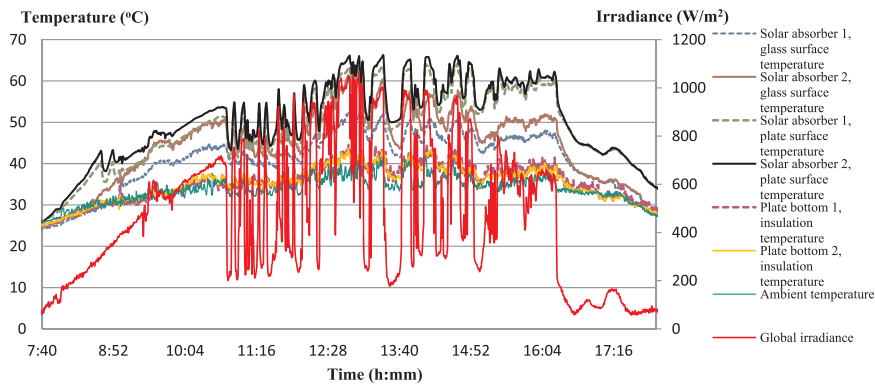


Fig. 4. Continuous daytime experimental data recording on 14 May 2016 under operating condition.

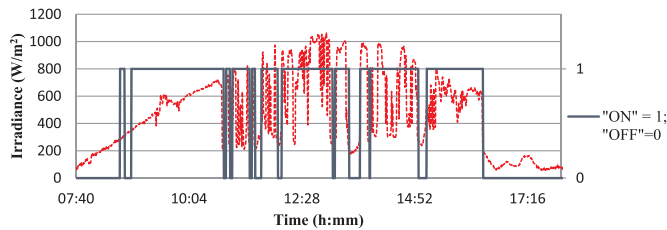


Fig. 5. Solar pump operation pattern on 14 May 2016.

flow was controlled automatically by a solar pump that associated with a standard solar collector system controller. The control setting for the pump was set: “ON” differential temperature set point at 8 °C and “OFF” differential temperature set point at 4 °C. The set points referred to the temperature difference between the solar absorber plate surface and storage tank. The setting is recommended by the manufacturer [22] which has also fulfilled the standard optimum setting given by [23,24]. Under the operating condition, the solar pump could circulate the water at a flow rate recorded at 5.08 L/min with a power consumption measured at 6.8 W. The volume of water in the storage tank was about 97.5 L/m² of absorber aperture area, which is within the recommended volume size for a standard solar hot water system [25]. Before starting the test, the storage tank was filled up with water. After one day test, the tank was drained, refilled and made ready before sunrise for the upcoming day test.

Measurement instruments employed in this experiment were data logger (DataTaker DT80), pyranometer (Eppley Radiometer Model 8–48), thermocouple sensors (Type-K), thermo anemometer (Model 9555 TSI VelociCalc), thermal infrared camera (Model FLIR E50), multimeter and flow meter. The trigger rate of data logging system was set to 30 s time interval. Time setting in the data logging device was set to the actual local clock time referring to the Malaysian Standard Time provided by [26]. The temperature field measurement was carried out

on the main parts of the experimental model such as glass top surface of solar absorber, plate surface of solar absorber, bottom of solar absorber and water inside storage tank. To verify the condition of the active direct solar heating system, a standard deviation analysis for four water temperature points measured at different water level inside the storage tank has been conducted. It indicated a low standard deviation at below 0.8 °C, showing that the thermal stratification did not exist in the storage tank as expected.

The performance of the system was evaluated referring to the global irradiance at the experimental site and the temperature measurements at several predefined points. These parameters were needed to investigate the system in the actual tropical sky. Measurements of the outdoor weather conditions were carried out as supporting data; i.e. relative humidity, wind speed and air temperature. These variables were not examined in this filed study; instead, they were employed to identify the ambient condition at the site. It was convenient to clarify in the early stage that the shading performance on improving indoor thermal comfort and thermal load reduction of a building was out of the scope in the present study. As an alternative to assess its capability of blocking thermal heat from entering a glazing opening, a thermographic imager was employed to measure the temperature distribution on the area beneath the system to evaluate the temperature mapping directly for the shaded and unshaded zones with evident outcome. In addition, a simulation outcome has been presented to verify the shading feature of the system. Fig. 3 illustrates the view of prototype at the experimental site.

The efficiency of a solar absorber is an important parameter to determine the thermal performance of a solar absorber system. In general, the efficiency is defined by the quotient of the useful gain over some specified time period to the incident solar energy over the same time period [27]. The actual daily efficiency of a solar thermal system at a site is formulated as [28–30],

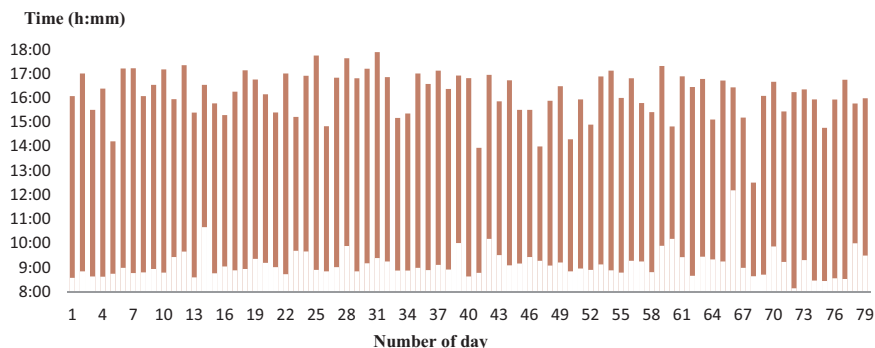


Fig. 6. Daily duration of solar heat collection from starting time to ending time for 79 sample days.

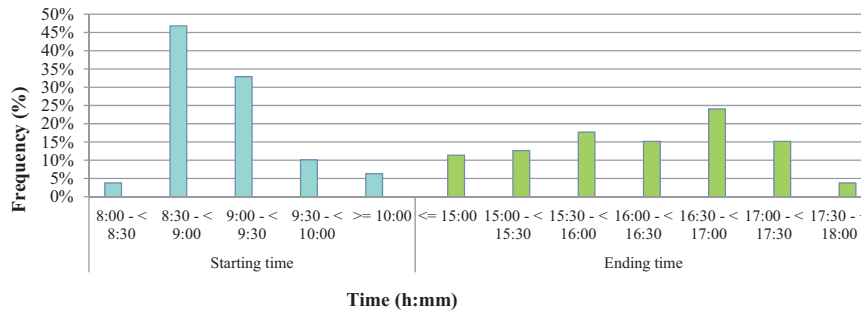


Fig. 7. Frequency of starting time and ending time for solar heat collection.

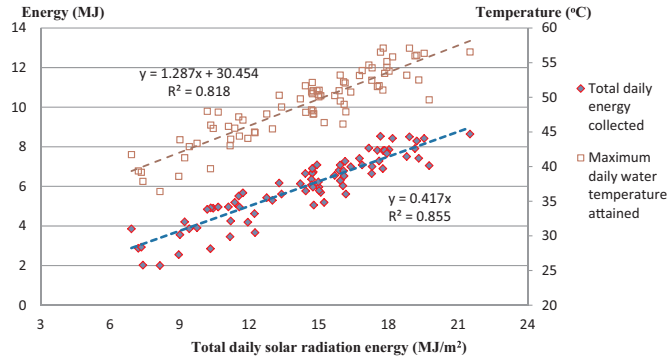


Fig. 8. Total daily energy collected and maximum daily water temperature attained in variation of total daily solar radiation energy received per unit area of collector.

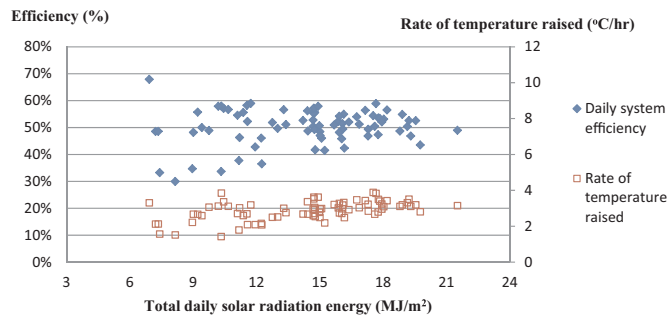


Fig. 9. Daily efficiency and rate of water temperature raised in variation of total daily solar radiation energy received by unit area of collector.

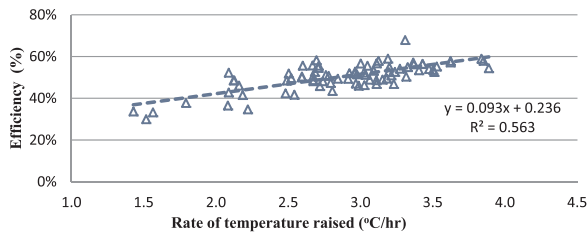


Fig. 10. Daily efficiency in variation of rate of temperature raised.

$$\eta = \frac{MC_p(T_F - T_I)}{A_c H_d} \quad (1)$$

where,

- η = Daily solar thermal system efficiency (%)
- M = Water mass in storage tank (kg)
- C_p = Specific heat of water (J/(kg K))
- T_F = Final temperature in storage tank after the test finishes (°C)
- T_I = Initial temperature in storage tank when the test starts (°C)

A_c = Area of solar absorber (m²)

H_d = Daily solar radiation of the test day (J/m²)

As the present work was intended for an actual outdoor field test with the use of standard system control mechanism, the test period for a daytime is defined by the on-site operation mode of the system, in which it would response to the site-related weather conditions.

3. Results and discussion

Fig. 4 shows a sample of experimental result that was recorded on 14 May 2016. The global irradiance on site was fluctuating due to the intermittent cloud blockages during the test period. From the presented pattern, the temperatures of the glass surface (cover) and plate surface were highly influenced by the solar radiation intensity at that instant. As the global irradiance increased, the temperatures of both the glass and plate surfaces increased and vice versa. In principle, the system was dependent and responsive to the available solar flux intensity as expected.

Fig. 5 presents the solar pump operation pattern regulated by the standard solar collector system controller on the same sample day. It depicted that the solar pump did not operate for one full daytime and would cease when the solar irradiance has dropped significantly for a relatively longer time. It has matched the nature of the irregular equatorial cloudy atmosphere in this field test. Due to the cloud formation, the solar radiation energy reaching on the ground was diminished. As the heat on the solar plate was transferred to the storage tank at the same time, it has subsequently caused the temperature drop of the plate surface. When it reached to the differential temperature set point of less than 4 °C, the operation was ceased, “OFF”. The solar pump would be resumed, “ON”, when the clear sky appeared again increasing the differential temperature equal to and greater than 8 °C. The control set points were found to be practical and crucial for cloudy weather to avoid high frequent starts and stops of the solar pump and concurrently retained the positive heat collection throughout a daytime.

The duration of solar heat collection of the system was observed to be dependent on the weather conditions at the site. Fig. 6 shows the daily duration of solar heat collection from starting time to ending time for all the 79 days during the test period. It could be seen that the starting and ending times for different days were varying in practice. Further analysis has been conducted to display the frequency of occurrence of the various starting times and ending times as presented in Fig. 7. The results showed that the system started to collect solar heat with recorded high frequency of occurrence up to 79.8% for one hour from 8:30 to before 9:30. The system was unlikely to operate before 8:30 with low occurrence recorded at merely 3.8%. It was due to the low grade of solar radiation intensity in the earlier morning which resulted longer time needed for preheating the system before it could gain the 8 °C temperature differential to trigger the solar pump. For the ending times, one could see a relatively flat profile for the frequency of occurrence. It was found that the system might stop to operate as earlier as before 15:00. It recorded that 56.9% of the operation of daytime solar heat collection was ceased before 16:30. The outcome showed that

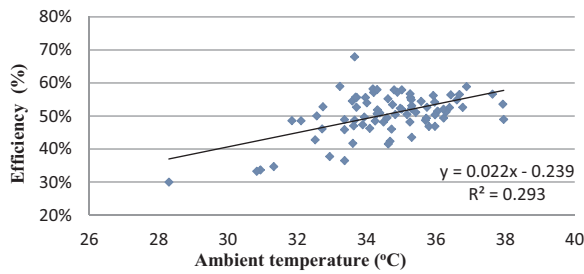


Fig. 11. Daily efficiency in variation of ambient temperature.

the site was exposed to the high occurrence of afternoon rain that has impaired the duration of the solar heat collection. It has revealed the actual outdoor solar heat collection pattern of the system under the influence of equatorial cloudy atmosphere. The scenario was different to other places having blue sky for a whole daytime.

Fig. 8 shows the results of the total daily energy collected and maximum daily water temperature attained in variation of total daily solar radiation energy received per unit area of collector. On average basis, with the total daily solar radiation energy received per unit collector area valued at 14.4 MJ/m^2 , the system was capable to collect and store 5.97 MJ of energy after one daytime operation with average maximum daily temperature attained at $48.9 \text{ }^\circ\text{C}$. During the test period, the lowest and highest daily total energy collected were 2.00 MJ and 8.64 MJ , respectively. After the daytime solar collection, the recorded lowest and highest daily water temperatures attainable were $36.4 \text{ }^\circ\text{C}$ and $57.1 \text{ }^\circ\text{C}$, respectively. The diagram shows that there exists a correlation between the recorded maximum daily water temperature attained and the total daily solar radiation energy received per unit area of collector in the present work. The maximum daily water temperature could be estimated using the linear equation with coefficient of determination (R^2) of 0.818 . The similar correlation was established for the total daily energy collected and the total daily solar radiation energy received per unit area of collector with $R^2 = 0.855$. The both linear regressions have indicated satisfactory correlation coefficient (R) valued 0.904 and 0.925 , respectively. It indicated the good relationships between these variables despite of the influence of irregular cloudy and solar radiation patterns on the system worked in the real operating mode.

Fig. 9 shows the effects of the total daily solar radiation energy received per unit area of collector on the daily efficiency and the rate of water temperature raised. In general, both the daily efficiency and rate of water temperature raised have depicted unobvious trends corresponded to the increase of total daily solar radiation energy received. It showed that the quantity of daily solar radiation energy in the tropical climates was less affecting the system efficiency; nevertheless, higher incident solar radiation energy could deduce the likelihood of getting higher system efficiency. From the results, the system could achieve 50.5% daily efficiency on average, with standard deviation of 6.5% . For the rate of water temperature raised, the system was able to heat up water at a rate of $2.9 \text{ }^\circ\text{C/h}$ on average, with standard deviation of

merely $0.5 \text{ }^\circ\text{C/h}$.

Due to the similar trend for both the daily efficiency and the rate of water temperature raised, there might be a relation existed between these two variables. Fig. 10 shows the relation between daily efficiency and rate of water temperature raised. The correlation indicated the R^2 and R to be 0.563 and 0.750 , respectively, which was fairly satisfactory in estimation of daily efficiency. The comparison study for the linear regression and the experimental values has shown a close discrepancy in calculating the daily efficiency with the deviation and the percentage difference computed at 3.4% and 6.9% , respectively.

Fig. 11 shows the effect of the ambient temperature on the daily efficiency. One could see that the relationship between the daily efficiency and the ambient temperature was weak, with $R^2 = 0.293$ and $R = 0.541$. It indicated that the ambient temperature was less influential to the daily efficiency of the present experimental model. Using this linear regression together with the measured data, a quantitative comparison can be conducted to verify the degree of discrepancy. The comparison indicated the tolerable deviation and the percentage difference valued at 4.5% and 9.6% , respectively. A t-test has been carried out to identify the significance of dependence for the measured data and the linear regression. The result showed that the calculated t-value was about -2.74 , which is greater than the critical t-value (1.99) at the alpha level of 0.05 . Thus, the null hypothesis that there is no different between the means of the measured data and the linear regression shall be rejected. This statistical test inferred that the proposed linear regression was unable to provide an accurate prediction for the daily efficiency by merely referring to the ambient temperature.

A detailed analysis has been carried out to reveal the frequency of occurrence of various daily efficiencies and maximum daily water temperatures attained by the system. Fig. 12 shows the patterns. The diagram showed that the system could perform at the daily efficiency ranging from 45% to 60% with recorded 84.8% of occurrence under the influence of hot tropical climate. In the aspect of maximum daily water temperature attained after one daytime solar heat collection, the results showed that 79.7% of occurrence was for temperature ranging from $45 \text{ }^\circ\text{C}$ to less than $60 \text{ }^\circ\text{C}$, indicating a satisfactory performance for the system in heating up the water with the volume of 97.5 L/m^2 . It should be noted that according to the field data, the highest water temperature attained was $57.1 \text{ }^\circ\text{C}$ with 54.9% daily efficiency. Besides, the average energy consumption of the solar pump for the solar heat harnessing process was merely 2.8% of the total thermal energy collected in the daily basis.

An additional experiment was carried out to check the heat distribution mapping of the system. Fig. 13 depicted the thermographic images on the top surfaces of the system, which illustrated a uniform surface temperature. Temperature gradient analysis along the straight lines following the water flow direction showed that the standard deviation was about $0.7 \text{ }^\circ\text{C}$ in average for both solar absorbers. To verify the outcome of the thermographic images, the standard deviation was computed for the three temperature points measured on each absorber plate surface using thermocouples, which indicated the average values of merely $0.6 \text{ }^\circ\text{C}$. From the thermographic images, the average temperature difference between the two solar absorbers was about $2.1 \text{ }^\circ\text{C}$.

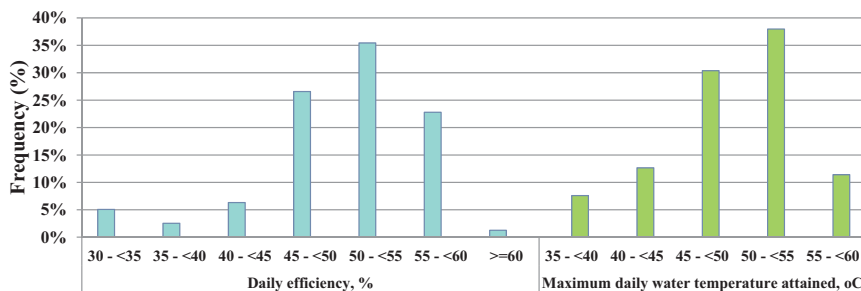


Fig. 12. Frequency of daily efficiency and maximum daily water temperature attained.

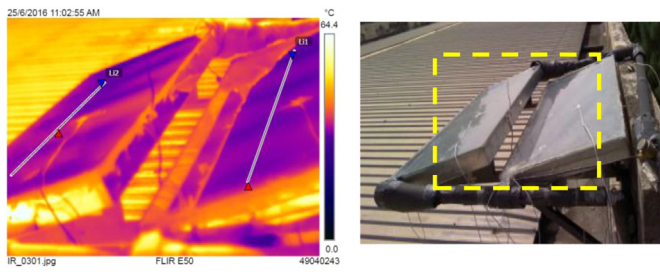


Fig. 13. Thermographic image of the shading façade-integrated solar absorber system.

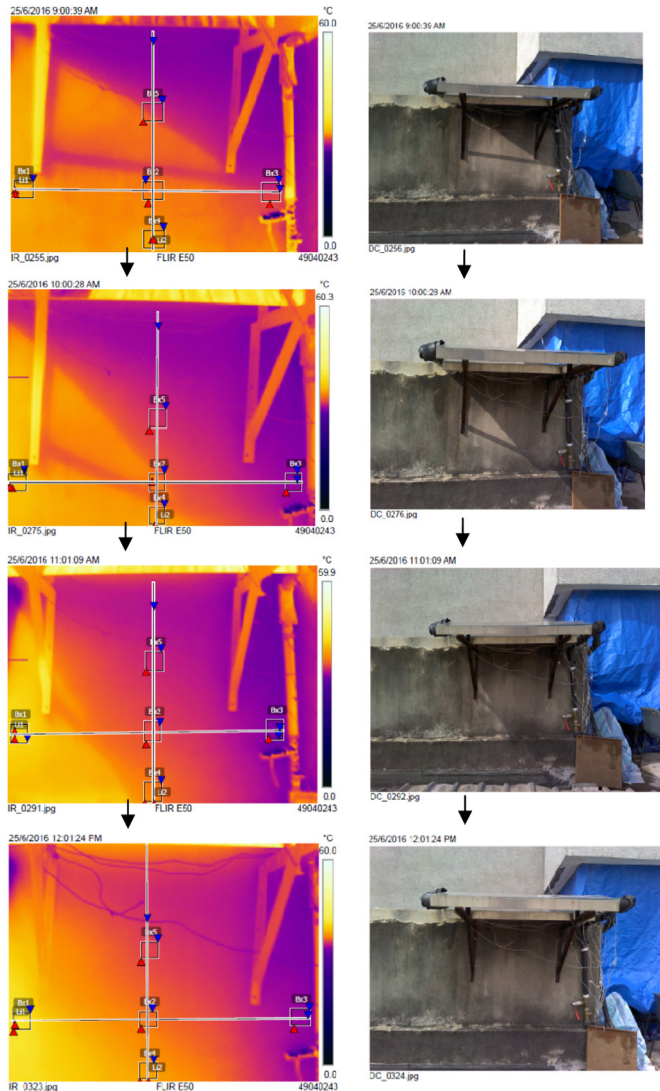


Fig. 14. Photographs and thermographic images of shaded and unshaded areas beneath shading façade-integrated solar absorber system on 25 June 2016 from 9:00 to 12:00.

Meanwhile, the measured temperature difference of absorber plate surface between the two solar absorbers was $1.5\text{ }^{\circ}\text{C}$ with standard deviation of $0.6\text{ }^{\circ}\text{C}$. It indicated that the temperature gradients presented by the thermographic images were in good agreements with the experimental data. The outcomes of the temperature gradient analysis along the water flow direction and the temperature difference between the two parallel solar absorbers are essential to verify the isothermal condition of the absorber plate and the uniformity of flow distribution for the parallel-flow configuration used in the system.

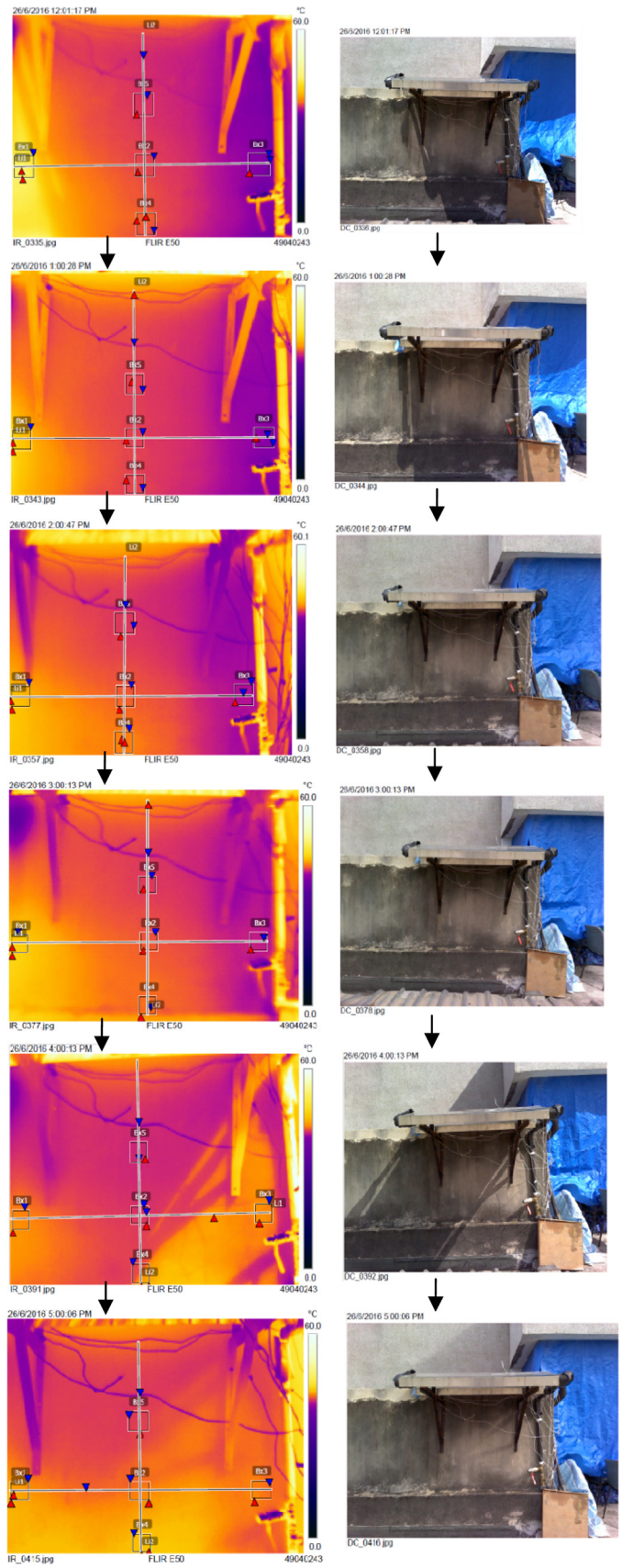


Fig. 15. Photographs and thermographic images of shaded and unshaded areas beneath shading façade-integrated solar absorber system on 26 June 2016 from 12:00 to 17:00.

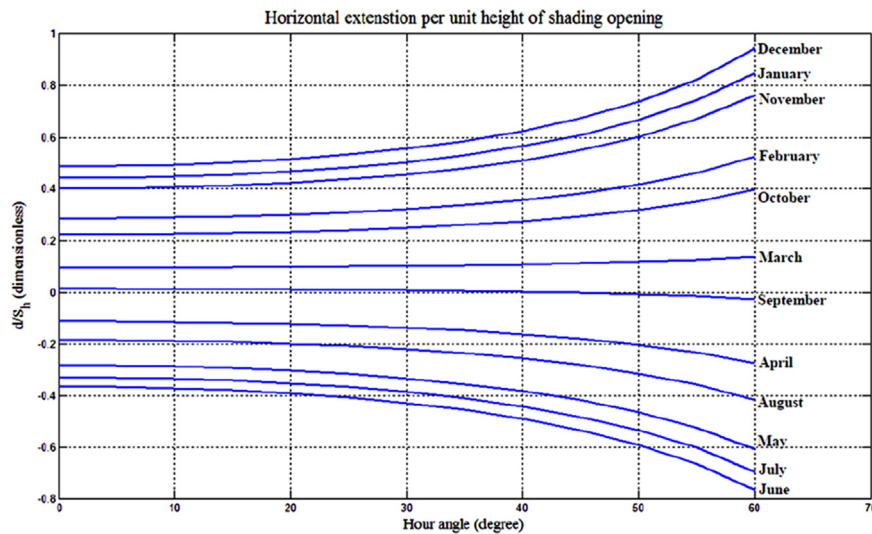


Fig. 16. Normalised horizontal extension, d/S_h .

Table 2
Normalised horizontal extension, d/S_h for different range of solar time and its corresponding horizontal extension dimensions for complete shading.

Solar time	Range of solar hour angle (deg.)	d/S_h , Normalised horizontal extension		Horizontal extension (mm)	
		South-facing shading	North-facing shading	South-facing shading	North-facing shading
08:00–16:00	0 → ± 60	0.9626	0.7806	1155	937
08:20–15:40	0 → ± 55	0.8410	0.6779	1009	813
08:40–15:20	0 → ± 50	0.7530	0.6020	904	722
09:00–15:00	0 → ± 45	0.6871	0.5443	825	653
09:20–14:40	0 → ± 40	0.6368	0.4998	764	600
09:40–14:20	0 → ± 35	0.5978	0.4650	717	558
10:00–14:00	0 → ± 30	0.5674	0.4377	681	525
10:20–13:40	0 → ± 25	0.5439	0.4165	653	500
10:40–13:20	0 → ± 20	0.5260	0.4002	631	480
11:00–13:00	0 → ± 15	0.5128	0.3882	615	466
11:20–12:40	0 → ± 10	0.5038	0.3800	605	456
11:40–12:20	0 → ± 5	0.4985	0.3751	598	450
12:00–12:00	0	0.4968	0.3736	596	448

The temperature mapping for the shaded and unshaded areas beneath the system was assessed by presenting the thermographic visualisation. Figs. 14 and 15 illustrate the photographs and thermographic images captured at the experimental site that showed the overall temperature distributions of shaded and unshaded zones from about 9:00 to 17:00 with one hour interval. From the temperature mapping, the shaded area recorded a noticeable lower temperature compared to the unshaded area due to the blockage of solar radiation by the system. Analysing the thermographic images, the temperature difference of the shaded and unshaded areas could possibly reach up to 9.7 °C, which implied the viability of the system to act as the shading device besides harnessing solar heat.

To further demonstrate the shading characterisation of the system, a computational simulation for sizing the horizontal extension (d) of the system per unit height of shaded opening below the horizontal shading façade (S_h), known as a normalised horizontal extension d/S_h , for the complete shading capacity up to 60° solar hour angle was presented. Fig. 16 shows the result. The figure consists of 12 curves corresponding to 12 months in one year. In this context, the curves with positive value refer to the façade extension for the south-facing side and the negative for the north-facing side. At the experimental site of the present work, the sun is at the lowest position on 21 December (south-facing shading)

and 21 June (north-facing shading) that require highest extension of shading. As the solar position deviates further from the zenith line due to the increment of solar hour angle, the larger extension is needed for the complete shading.

The d/S_h for different range of solar time and its corresponding horizontal extension dimensions for complete shading are tabulated in Table 2. Using a typical and common residential building’s window dimension of 600 mm (width) × 1200 mm (height) as a reference, the exact dimension of horizontal extension for the system model could be computed. It was determined based on the solar time interval from 09:00 to 15:00, corresponding to the solar hour angle of ± 45°. This duration is adequate corresponding to the overheated time frame with high solar intensity in tropics. From the result, the required horizontal extension for complete shading feature throughout a year was 825 mm, in which the size could be standardised for both south and north orientations. With a marginally larger size of the horizontal extension of the prototype at 864 mm, the shading façade-integrated solar absorber system in the present work could act as the shading unit satisfactorily.

4. Conclusions

In this work, the outdoor performance of the shading façade-integrated solar absorber system operated under the hot tropical climate has been investigated. From the experimental results, the system was principally dependent on the available global irradiance. Under the operating condition in the real sky of tropical area, the system was probably to operate started from 8:30 to before 9:30 and ceased at anytime of postmeridian period as earlier as before 15:00. It was caused by the high occurrence of afternoon rain at the experimental site. During the test period, the system was capable to collect and store 5.97 MJ of energy after one daytime operation with the average daily solar radiation energy received per unit collector area valued at 14.4 MJ/m². Detailed results showed that the system could perform at the daily efficiency ranging from 45% to 60% and maximum daily temperature attained from 45 °C to less than 60 °C with recorded high percentages of occurrences. From the field data, the highest water temperature attained was 57.1 °C with 54.9% daily efficiency. On average basis, the system could achieve 50.5% daily efficiency and solar water heating rate of 2.9 °C/h.

The result depicted that the elevated solar radiation energy received per unit area of collector could induce higher energy collected and increased water temperature attained by the system. Empirical result showed that there existed a good correlation between the total daily energy collected and the total daily solar radiation energy received per

unit area of collector with $R^2 = 0.855$. Besides, a linear regression has been developed for the maximum daily water temperature attained and the total daily solar radiation energy received per unit area of collector with $R^2 = 0.818$. From the both empirical results, the daily energy collected and the maximum daily water temperature attained by the system could be approximated satisfactorily by knowing the daily solar radiation energy received per collector area. Meanwhile, the daily efficiency and rate of water temperature raised have depicted unobvious trends corresponded to the increase of the daily solar radiation energy received. The experimental result showed that the ambient temperature was less influential to the daily efficiency, in which the statistical t-test inferred that the proposed linear regression between the ambient temperature and the daily efficiency could not be employed as a predictive model. Further analyses were conducted to verify the isothermal condition of absorber plate and uniformity of flow distribution. The additional experiment has verified the system as a shading unit besides its capability of harnessing solar heat.

The outcomes have revealed the positive potential of the presently developed shading façade-integrated solar absorber in harnessing incident solar energy for thermal applications, which could serve as a general reference for the solar application in buildings under the hot tropical climate with equatorial cloudy atmosphere. For future work, investigation in overall energy saving could be conducted by incorporating the analysis of building energy saving to quantify the thermal load reduction by the system.

Acknowledgements

Funding for this work was provided by “Geran Universiti Putra Malaysia” Project code: GP-IPS/2014/9438707. The first author would like to acknowledge the Ministry of Higher Education Malaysia for the MyBrain15-MyPhD scholarship.

References

- [1] V.V. Tyagi, D. Buddhi, R. Kothari, S.K. Tyagi, Phase change material (PCM) based thermal management system for cool energy storage application in building: an experimental study, *Energy Build.* 51 (0) (2012) 248–254.
- [2] A.A. Al-Abidi, S. Bin Mat, K. Sopian, M.Y. Sulaiman, C.H. Lim, A. Th, Review of thermal energy storage for air conditioning systems, *Renew. Sustain. Energy Rev.* 16 (8) (2012) 5802–5819.
- [3] D.-C. Chou, C.-S. Chang, J.-C. Chang, Energy conservation using solar collectors integrated with building louvre shading devices, *Appl. Therm. Eng.* 93 (2016) 1282–1294.
- [4] D. Chemisana, J. Lopez-Villada, A. Coronas, J.I. Rosell, C. Lodi, Building integration of concentrating systems for solar cooling applications, *Appl. Therm. Eng.* 50 (2) (2013) 1472–1479.
- [5] F. Motte, G. Notton, C. Cristofari, J.-L. Canaletti, A building integrated solar collector: performances characterization and first stage of numerical calculation, *Renew. Energy* 49 (0) (2013) 1–5.
- [6] F. Motte, G. Notton, C. Cristofari, J.-L. Canaletti, Design and modelling of a new patented thermal solar collector with high building integration, *Appl. Energy* 102 (0) (2013) 631–639.
- [7] Y. Yang, Q. Wang, D. Xiu, Z. Zhao, Q. Sun, A building integrated solar collector: all-ceramic solar collector, *Energy Build.* 62 (0) (2013) 15–17.
- [8] D. Xuan, H. Yajing, H. Jiang, The integrated design of SWH systems in high-rise buildings for hot-summer and warm-winter climates: Analysis of heat-collecting performanc of the integrated solar system, in: *Proceedings of the 2012 2nd International Conference on Consumer Electronics, Communications and Networks (CECNet)*, 2012.
- [9] S. Mekhilef, A. Safari, W.E.S. Mustaffa, R. Saidur, R. Omar, M.A.A. Younis, Solar energy in Malaysia: current state and prospects, *Renew. Sustain. Energy Rev.* 16 (1) (2012) 386–396.
- [10] M. D’Antoni, O. Saro, Massive solar-thermal collectors: a critical literature review, *Renew. Sustain. Energy Rev.* 16 (6) (2012) 3666–3679.
- [11] A.K. Furundzic, V. Kosoric, K. Golic, Potential for reduction of CO₂ emissions by integration of solar water heating systems on student dormitories through building refurbishment, *Sustain. Cities Soc.* 2 (1) (2012) 50–62.
- [12] M. Mandalaki, K. Zervas, T. Tsoutsos, A. Vazakas, Assessment of fixed shading devices with integrated PV for efficient energy use, *Sol. Energy* 86 (9) (2012) 2561–2575.
- [13] L.L. Sun, H.X. Yang, Impacts of the shading-type building-integrated photovoltaic claddings on electricity generation and cooling load component through shaded windows, *Energy Build.* 42 (4) (2010) 455–460.
- [14] A.I. Palmero-Marrero, A.C. Oliveira, Evaluation of a solar thermal system using building louvre shading devices, *Sol. Energy* 80 (5) (2006) 545–554.
- [15] A.I. Palmero-Marrero, A.C. Oliveira, Evaluation of a solar louvre collector system for building heating and cooling, *Int. J. Ambient Energy* 29 (2) (2008) 59–64.
- [16] A.M. Abu-Zour, S.B. Riffat, M. Gillott, New design of solar collector integrated into solar louvres for efficient heat transfer, *Appl. Therm. Eng.* 26 (16) (2006) 1876–1882.
- [17] A.I. Palmero-Marrero, A.C. Oliveira, Testing of an integrated solar louvre collector, *Int. J. Ambient Energy* 25 (4) (2004) 171–176.
- [18] M. Mandalaki, T. Tsoutsos, N. Papamanolis, Integrated PV in shading systems for Mediterranean countries: balance between energy production and visual comfort, *Energy Build.* 77 (2014) 445–456.
- [19] J. Ji, C. Luo, T.-T. Chow, W. Sun, W. He, Thermal characteristics of a building-integrated dual-function solar collector in water heating mode with natural circulation, *Energy* 36 (1) (2011) 566–574.
- [20] T. Salem, P. Michel, Experimental study of active solar thermal collectors integrated in building facade, in: *Proceedings of ISES World Congress 2007 (Vol. 1–Vol. V)*, D. Y. Goswami and Y. Zhao, Editors, Springer Berlin Heidelberg, 2009. p. 332–336.
- [21] M. Ramirez-Stefanou, T. Mallick, M. Smyth, J.D. Mondol, A. Zacharopoulos, T.J. Hyde, Characterisation of a line-axis solar thermal collector for building facade integration, in: R. Howlett, L.C. Jain, S.H. Lee (Eds.), *Sustainability in Energy and Buildings*, Springer Berlin Heidelberg, 2011, pp. 277–287.
- [22] MISOL International, Installation and Operating Manual: SR868C8/SR868C8Q Solar Controller, MISOL International E-Commerce, China, 2012.
- [23] ASHRAE, ASHRAE Handbook - HVAC Systems and Equipment 2008 The American Society of Heating, Refrigerating and Air-Conditioning Engineers, Atlanta, 2008.
- [24] S.A. Kalogirou, Chapter five – Solar Water Heating Systems, *Solar Energy Engineering*, Academic Press, Boston, 2009, pp. 251–314.
- [25] ASHRAE, ASHRAE Handbook – HVAC Applications 2007 The American Society of Heating, Refrigerating and Air-Conditioning Engineers, Atlanta, 2007.
- [26] SIRIM Malays. Stand. Time 2016. (cited 2016 19 April). Available from <<http://mst.sirim.my/>>.
- [27] J.A. Duffie, W.A. Beckman, *Solar Engineering of Thermal Processes*, Third ed., John Wiley & Sons, Inc, Hoboken, NJ, 2006.
- [28] N. Roonprasang, P. Namprakai, N. Pratinthong, Experimental studies of a new solar water heater system using a solar water pump, *Energy* 33 (4) (2008) 639–646.
- [29] M. Souliotis, D. Chemisana, Y.G. Caouris, Y. Tripanagnostopoulos, Experimental study of integrated collector storage solar water heaters, *Renew. Energy* 50 (2013) 1083–1094.
- [30] X. Zhang, S. You, W. Xu, M. Wang, T. He, X. Zheng, Experimental investigation of the higher coefficient of thermal performance for water-in-glass evacuated tube solar water heaters in China, *Energy Convers. Manag.* 78 (2014) 386–392.